Cost-Effective Airborne SAR

D. M. Vavriv, V. V. Vynogradov, V. A. Volkov, R. V. Kozhyn,
O. O. Bezvesilniy, S. V. Alekseenkov, A. V. Shevchenko, A. A. Belikov,
M. P. Vasilevskiy, and D. I. Zaikin

Institute of Radio Astronomy, NAS Ukraine,
4, Chervonopraporna st., Kharkiv, 61002, Ukraine
E-mail:vavriv@rian.kharkov.ua

A Ku-band airborne SAR, which is a cost effective system in terms of the development and exploitation costs, has been recently developed and tested at the Institute of Radio Astronomy of the National Academy of Sciences of Ukraine. The SAR system is capable of producing real-time, high-resolution images, and it can be effectively operated from light weight aircrafts. The system benefits essentially from the introduction of a novel algorithm of a real-time estimation of the aircraft orientation angles, which is based on the analysis of backscattered signals. This paper describes the principles of the SAR operation, the setup of the SAR system, its main components, and the signal processing technique used. The results obtained during flight tests are summarized as well.

1. Introduction

Synthetic aperture radar (SAR) systems are recognized now as the most effective instruments for high resolution mapping of earth surfaces and for other related applications [1-3]. Up to now, several dozens of SAR systems operated from spaceborne and airborne platforms have been put into exploitation. One of the promising directions of the further extension of SAR applications is related with the development of cost effective systems which can be operated from light weight aircraft [4-6]. Having a real-time signal processing option as well as a rapid deployment, such systems are very much needed, for example, to monitor disaster areas. However, until recently, the application of light-weight airborne platforms has been seriously limited by the problem of an accurate estimation of the platform orientation angles which should be known in real time in order to produce high quality images [7-10]. The solutions, which are used for this purpose in case of heavy aircrafts and satellites, have appeared to be not accurate enough and, besides, they are rather expensive. We

have proposed [5] a radical solution to this problem, which is based on the estimation of the aircraft orientation angles directly from radar returns. This solution has been tested with a squinted SAR operated from a light-weight aircraft and it has demonstrated a high efficiency and robustness [4]. The application of the proposed technique enables us to use a simple navigation system consisting of a radar altimeter and a single GPS receiver only.

We have also used some other solutions in order to make the system cost effective. In particular, a high range resolution has been achieved by using the pulse compression technique with binary phase coding of transmitted pulses. The application of such pulse compression instead of the conventionally used frequency sweeping technique reduces requirements to the digital signal processing system and enables the realization of real-time signal processing easily.

We also introduced and implemented a specific pre-filtering procedure to enable an accurate range migration correction for the squinted SAR mode accounting for the dependence of the Doppler centroid on range.

Possible areas of the application of the developed system have been extended by introducing a moving target indication technique and a capability to perform measurements at two linear orthogonal polarizations.

In this paper, we describe the principles of the SAR operation, the setup of the developed SAR system with the focus on the proposed technique of the estimation of the aircraft orientation angles directly from radar returns. Main components and the signal processing technique used in the system are presented as well. The results obtained during flight tests are also summarized. The paper is organized as follows: In Section 2, we give a review of basic principles of the radar operation. This section can be considered as a short tutorial of the SAR operation. The method of the estimation of the aircraft orientation angles is presented in Section 3. In Section 4, a novel autofocusing technique, which is used for post-processing of SAR images, is described. Section 5 gives a description of the radar hardware, and Section 6 contains the results obtained during flight tests.

2. Basic Principles of the SAR Operation

2.1. Pulse Compression in Range

The described SAR system has true coherent processing scheme, the transmitter is based on TWT operating in the amplification regime. The transmitted peak power is $P_P = 100$ W, and to provide the required mean power the long pulses of duration $\tau_P = 5$ μs are transmitted. The pulse compression based on binary phase coding is used in the discussed SAR system to obtain the high range resolution of $\rho_R = 3$ m. The phase-coded pulse bandwidth B_{CP} and the duration of the compressed pulse τ_{CP} are related by

$$B_{CP} = 1/\tau_{CP}.$$

If τ_P denotes the duration of the long pulse, then the compression ratio can be written as a product of the pulse bandwidth and the pulse duration:

$$K_R = \tau_P/\tau_{CP} = B_{CP}\tau_P. \tag{1}$$

The effective power of the compressed pulse is greater than the power of the long pulse by a factor K_R: $P_{CP} = K_R P_T$. In the described SAR system, the compression ratio is $K_R = 255$ and, consequently, the effective peak power is $P_{CP} = 25.5$ kW, and the slant range resolution is $\rho_R = c\tau_{CP}/2 = c\tau_P/(2K_R) = 3$ m. The sampling frequency in the slant range is 100 MHz, which corresponds to a 1.5 m sampling.

There are two mostly used pulse compression techniques: linear frequency modulation (FM) (also known as "chirp") [11] and phase coding [11, 12]. The advantage of FM pulses is related to a possibility to achieve a rather low side-lobe level. However, in this case, any practical pulse compression algorithm (complex convolution) involves a number of complex multiplications, increasing the cost and complexity of the processing system.

In case of the pulse compression based on the phase coding, the phase inside of a long pulse is changed repeatedly by π according to some binary sequence, called the code sequence. Therefore the reference waveform in the convolution takes values –1 or +1 only, and the multiplications in the convolution are replaced by summations or subtractions, resulting in a more effective computational algorithm, which can be easily implemented in the digital hardware.

In the discussed SAR system, we have used the PN-sequences (also called M-sequences) [13] of the length of 255. The side-lobe level of the compressed pulse coded with such sequence is –22.5 dB, limiting the dynamic range of radar images. An important property of the M-sequences is that the circular shifted sequences (that yields 255 different sequences) give practically uncorrelated side-lobes. To decrease the side-lobes, we change coding sequence in random order from pulse to pulse. In such a way, after a pre-filtering procedure and the azimuth synthesis we achieve the side-lobe level in a range as small as –34.5 dB.

2.2. Strip-Map Synthetic Aperture Technique

The synthetic aperture technique is used in order to get a high along track resolution by using a physically small antenna. This is achieved via collecting and processing the radar backscattering signals during some time. We are considering a strip-map mode of operation, when the radar antenna beam illuminates a strip on the ground surface, which is almost parallel to the flight trajectory. Provided that the antenna beam width is θ_A, the distance from the antenna phase center to the target is R, and V is the plane velocity, one can find that the maximum illumination time of a point like target, called the time of synthesis, is

$$T_S = R\theta_A/V, \qquad (2)$$

under the condition that the antenna beam is oriented perpendicularly to the flight trajectory. This is the case of so called non-squint SAR. The term "squint mode" means that the antenna beam direction is not in general perpendicular to the fight trajectory.

Let us derive the main relations governing the signal processing for the strip-map SAR. In the ideal case, the strip-map mode implies that the aircraft (or, more precisely, the phase centre of the transmitting-receiving antenna) moves along a straight line with a constant velocity at a fixed height, and with the antenna beam pointed exactly across the line of flight. In real flight conditions, all of the above mentioned idealizations are incorrect, especially for small aircrafts. In the general case, the antenna beam orientation can deviate from the perpendicular side-look direction and the trajectory is in general curved.

The orientation of the antenna beam is described by three angles: the pitch angle, α, the yaw angle, β, and the roll angle, γ, which are the angles of the three consequent rotations around axes of the airborne coordinate system (however, with the origin shifted to the phase centre of the antenna), which turn the antenna beam from the side-looking, transverse direction to another one. The con-

sequent rotations are 1) around the pitch axis, which goes parallel to the aircraft wings; 2) around the yaw axis, which is perpendicular to the pitch and roll axes; 3) around the roll axis, which goes from the tail to the nose of the aircraft. The roll angle determines only the antenna elevation diagram position with respect to range samples, but it does not affect the mean Doppler frequency of the reflected signals, which is also known as the Doppler centroid. If the pitch and/or the yaw angles are non-zero, the antenna beam will be pointed forward or backward from the direction across the line of flight, and thus the received backscattered signals will have a non-zero Doppler centroid. It is supposed hereinafter that the orientation angles are changed slowly, and that they can be considered as constant during the time of synthesis.

The strip-map mode SAR geometry is illustrated in Fig. 2.1. We use a local coordinate system with the axes x and y, placed on the Earth surface, and with the z-axis which goes through the antenna centre. At each moment of time, the x-axis is oriented along the horizontal component of the flight vector.

The vector $\mathbf{R} = (x_R, y_R, -H)$, where H is the flight altitude, is the slant range from the antenna center to the point (x_R, y_R) on the line which is the intersection of the ground plane with the antenna elevation plane. The equation of this line is given by
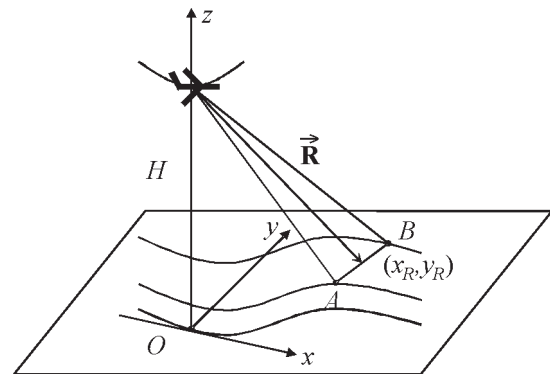

Fig. 2.1. *General case of the strip-map mode SAR geometry*

$$y_R = (x_R - H\tan\alpha/\cos\beta)/\tan\beta. \qquad (3)$$

If we know the slant range R to the point (x_R, y_R) on this line, then the coordinates of this point are given by

$$x_R = (H\tan\alpha)\cos\beta + \sin\beta\sqrt{R^2 - H^2 - (H\tan\alpha)^2}, \qquad (4a)$$

$$y_R = -(H\tan\alpha)\sin\beta + \cos\beta\sqrt{R^2 - H^2 - (H\tan\alpha)^2}. \qquad (4b)$$

At any given point, the trajectory can be approximated by parabolas

$$x(t) = V_x t + A_x t^2/2,$$
$$y(t) = V_y t + A_y t^2/2, \qquad (5)$$
$$z(t) = H + V_z t + A_z t^2/2,$$

where t belongs to the synthesis interval (2): $-T_S/2 \le t \le T_S/2$, and V_x, V_y, V_z and A_x, A_y, A_z are the components of the velocity, $\mathbf{V}$, and acceleration, $\mathbf{A}$, respectively.

Under this approximation, the slant range to a target at the point (x_R, y_R) in the interval of synthesis is given by

$$R(t) = \left[\left(x_R - V_x t - A_x t^2/2 \right)^2 + \left(y_R - V_y t - A_y t^2/2 \right)^2 + \right.$$
$$\left. + \left(-H - V_z t - A_z t^2/2 \right)^2 \right]^{1/2}. \qquad (6)$$

Taking into account that $V_y = 0$ because at each moment the x-axis is oriented along the horizontal component of the flight vector, the above relation (6) for the slant range can be written as:

$$R(t) \approx \sqrt{R^2 - 2(\mathbf{R}\cdot\mathbf{V})t + \left[V^2 - (\mathbf{R}\cdot\mathbf{A}) \right]t^2} \approx$$
$$\approx R - \frac{(\mathbf{R}\cdot\mathbf{V})}{R}t + \left[\frac{V^2}{R} - \frac{(\mathbf{R}\cdot\mathbf{V})^2}{R^3} - \frac{(\mathbf{R}\cdot\mathbf{A})}{R} \right]\frac{t^2}{2}, \qquad (7)$$

where $R = |\mathbf{R}|$ and $V = |\mathbf{V}|$. The instantaneous Doppler frequency of backscattered radar signal is given by

$$f(t) \equiv -\frac{2}{\lambda}\frac{dR(t)}{dt} = \frac{2}{\lambda}\frac{(\mathbf{R}\cdot\mathbf{V})}{R} -$$
$$-\frac{2}{\lambda}\left[\frac{V^2}{R} - \frac{(\mathbf{R}\cdot\mathbf{V})^2}{R^3} - \frac{(\mathbf{R}\cdot\mathbf{A})}{R} \right]t. \qquad (8)$$

It is convenient to write this frequency in terms of the Doppler centroid, F_{DC}, and the Doppler frequency rate, F_{DR}, as

$$f(t) = F_{DC} + F_{DR}t,$$

where

$$F_{DC} = \frac{2}{\lambda}\frac{(\mathbf{R}\cdot\mathbf{V})}{R},$$

$$\qquad (9)$$

$$F_{DR} = -\frac{2}{\lambda}\left[\frac{V^2}{R} - \frac{(\mathbf{R}\cdot\mathbf{V})^2}{R^3} - \frac{(\mathbf{R}\cdot\mathbf{A})}{R} \right].$$

Thus, as one can see from (4) and (9), in the strip-map mode, both the Doppler centroid and the Doppler rate depend on the pitch and yaw angles α and β, and on the slant range, so that signal processing is complicated considerably.

The synthesis of the aperture is equivalent to the linear FM pulse compression by applying the matched filter in time domain. The synthesized aperture $I(t)$ is obtained as a convolution in time domain of the received radar return, $s(t)$, with the reference function of the matched filter, $h(t)$. Here the reference function is given by

$$h(t) = w_H(t)\exp\left[-2\pi i\left(F_{DC}t + F_{DR}t^2/2 \right) \right],$$

where $w_H(t)$ is a weighting window, and thus

$$I(t) = \left| \frac{1}{T_S} \int\limits_{-T_S/2}^{T_S/2} s(t+t')h(t')\mathrm{d}t' \right|^2. \qquad (10)$$

Usually, the normalized Hamming window

$$w_H(t) = 1 + \frac{23}{27}\cos\left(2\pi t/T_S\right),$$

$$\left| \frac{1}{T_S} \int\limits_{-T_S/2}^{T_S/2} w_H(t)\mathrm{d}t \right|^2 = 1$$

is used to reduce the side-lobes of the synthetic aperture pattern.

The synthetic aperture diagram can be calculated from (10) by substituting the single point target return as a received signal:

$$I_{AP}(t) = \left| \frac{1}{T_S} \int\limits_{-T_S/2}^{T_S/2} s_{PT}(t+t')h(t')\mathrm{d}t' \right|^2 =$$

$$= \left| \frac{1}{T_S} \int\limits_{-T_S/2}^{T_S/2} \exp\left[i2\pi\left(F_{DC}(t+t') + F_{DR}(t+t')^2/2 \right) \right] \times \right.$$

$$\left. \times w_H(t')\exp\left[-i2\pi\left(F_{DC}t' + F_{DR}t'^2/2 \right) \right]\mathrm{d}t' \right|^2 =$$

$$= \left| \frac{1}{T_S} \int\limits_{-T_S/2}^{T_S/2} \left[1 + (23/27)\cos\left(2\pi t'/T_S \right) \right] \times \right.$$

$$\left. \times \exp\left[i2\pi F_{DR}tt' \right]\mathrm{d}t' \right|^2 = \left(\frac{\sin\left(\pi F_{DR}T_S t \right)}{\pi F_{DR}T_S t} \right)^2 \times$$

$$\times \left[\frac{1 - (F_{DR}T_S t)^2 (4/27)}{1 - (F_{DR}T_S t)^2} \right]^2. \qquad (11)$$

One can find that the synthesized aperture pattern (11) takes exactly the half of its maximum value for $t = \pm t_{1/2}$:

$$I\left(\pm F_{DR}T_S t_{1/2} \right) = 1/2, \qquad F_{DR}T_S t_{1/2} \approx 0.6515.$$

Therefore, for the azimuth resolutions, ρ_x, we can write:

$$\rho_x = V_x \cdot 2t_{1/2} \approx 1.3 \cdot \frac{V_x}{|F_{DR}|T_S}. \qquad (12)$$

Taking into account (2) and (12), the coefficient of the azimuth pulse compression can be introduced as:

$$K_A = \frac{L_S}{\rho_x} = B_A T_S, \qquad (13)$$

where $L_S = V_x T_S$ is the synthesis length and $B_A = F_{DR}T_S/1.3$ is the azimuth response signal bandwidth. The coefficient 1.3 is only due to the weighting Hamming window used here. Similar to the range pulse compression (1), the azimuth compression ratio (13) is a product of the azimuth pulse bandwidth and the azimuth pulse duration. This is one of the basic relations in the SAR technique and it does not depend on the type of signal coding.

From the theoretical point of view, the antenna aperture synthesizing (the azimuth pulse compression) is a somewhat simplier task, when the orientation of the radar platform is not changed and the aircraft moves uniformly along a straight horizontal line with a constant velocity at a fixed height. In practice, these conditions are never fulfilled, especially for the airborne radar systems installed on light weight aircrafts.

Variations of the aircraft velocity components and the aircraft attitude angles exert a strong effect on the reference function (also called the single point function response – SPRF) in the synthesizing filter (10). This leads to a necessity to compensate these variations in real time, as it will be discussed in Section 3.

Besides that, as the antenna ground footprint position depends on the aircraft attitude angles, the range migration effect increases. While an aircraft is flying over a ground target, the target is moving through the antenna footprint, the slant range to the

target is changed and it can cross several range gates. This behavior is called the range migration. To achieve a high azimuth resolution, the range migration should be properly accounted and compensated, because it is necessary to synthesize the signal from a target during the whole time while it is illuminated by the antenna beam. This means that the one-dimensional signal required for the aperture synthesis (10) should be sampled from a 2D-array of IQ-signals "range-azimuth" with the corresponding interpolation (see Section 2.4 for details).

2.3. Moving Target Detection

Ground moving target detection and indication (MTI) with SAR is generally a separate and difficult task. The problem is related with the fact that the filter which performs the synthesis of the aperture, for any realization of the filter, is designed to match the signals scattered from the terrain and ground stationary targets. Fast moving targets with considerable radial (line-of-sight) velocity components could not be seen in SAR images because their Doppler frequencies can be beyond the pass band of the synthesized filter. Slowly moving targets, whose Doppler frequencies are within the pass band of the filter (usually the pass band of the filter fits the Doppler bandwidth of the terrain signal) can be seen in SAR images. However, even detection of slowly moving targets is not an easy task, because of several problems. Firstly, the image of such a target can suffer from considerable radiometric distortion. Secondly, the moving target appears shifted from its true positions in the SAR image because of its own radial Doppler velocity. Finally, the image of the moving target can be defocused due to its own along-track (azimuthal) velocity [14].

To detect and indicate slowly moving ground targets, whose Doppler frequencies are within the Doppler bandwidth of the terrain (clutter) signal, the displaced phase center antenna (DPCA) method [15] or the along-track interferometry (ATI) technique [16-18] are commonly used. The idea of these methods consists in the following. By using two

antennas (for DPCA or ATI) or one antenna with two phase centers (for DPCA), which are separated in the along-track (azimuthal) direction, it is possible to perform imaging of the same terrain patch twice from the same point of the trajectory of the SAR platform with a time delay. Then, by comparing the signals from two receiving channels, a filter can be built for clutter suppression and moving target detection. The methods call for using two antennas or one sophisticated antenna with two phase centers (switchable phase array or monopulse antenna), and implementing two receiving channels, so that the cost of the radar system increases. The problem of the synchronization of the two receiving channels in time and space also arises, complicating the signal processing tasks and imposing additional constraints on the radar operating modes and the radar hardware.

Nowadays, the space-time adaptive processing (STAP) is also being developed rapidly and considered as the most powerful method for clutter suppression and moving target detection [19-21]. However, the STAP technique calls for a phase array antenna and a multi-channel receiver and provides a huge computational load on the radar processing system.

In practice, fast moving targets are also of interest. In the described SAR system, moving targets with radial velocities greater than ± 0.5 m/s, which are equivalent to the Doppler shift of ± 50 Hz at Ku-band, are required to be detected and indicated. In the SAR system, the antenna length and, consequently, the antenna beam width in the along-track direction, were chosen to provide the Doppler bandwidth of the terrain (clutter) of 100 Hz, by taking into account the maximum aircraft flight velocity. This has allowed us to use the simplest method of moving target detection – by detecting radar returns with Doppler frequencies beyond the bandwidth of clutter [15]. Typical dynamic Doppler spectrum of such a target along with a ground clutter is shown in Fig. 2.2. In this approach, the azimuthal resolution for moving targets is determined by the beam width of the real antenna, which is
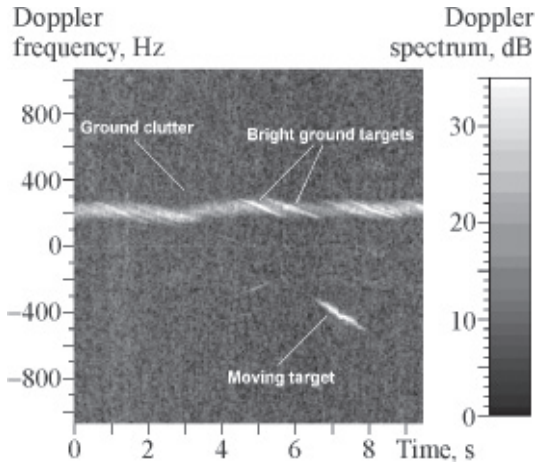
Fig. 2.2. *Dynamic Doppler spectrum with ground clutter and moving target*

Fig. 2.3. *Doppler spectrum with ground clutter and moving target*

worse then the azimuth resolution provided by the synthetic aperture for stationary targets and terrain. However, taking into account that a moving target appears on several consequent Doppler spectra (up to 10) during the time of synthesis, the azimuthal position of the moving target can be improved by finding the spectrum with the maximum power. Thus the single antenna and the single-channel receiver are used in the described SAR, making the introduced MTI technique simple and inexpensive in comparison to other MTI techniques. However, this realization does not allow detecting and indicating slowly moving targets in clutter.

In the described radar, the Doppler spectra in the azimuthal direction are calculated for all range gates after the range compression, but before the pre-filtering. An example of the Doppler spectrum with a moving target is shown in Fig. 2.3. The part of the spectrum, which appears above the noise and which is different from the Doppler spectrum of clutter (with the known Doppler centroid) indicates the presence of a moving target. The mean radial velocity of the target can be estimated. The minimal detectable radial velocity is 0.54 m/s, and the unambiguous range of the radial Doppler velocities is from –100 m/s to +100 m/s. The accuracy of the velocity measurement is about 0.2 m/s.
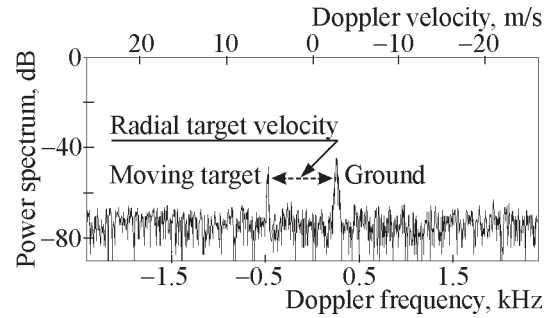
2.4. Range Migration Correction and Pre-Filter Design

While an airborne or spaceborne SAR is moving along its trajectory, the slant range to a target according to (7)–(9) changes as

$$R(t) \approx R + \frac{\lambda}{2} F_{DC} t + \frac{\lambda}{2} F_{DR} \frac{t^2}{2}. \qquad (14)$$

When the distance to the target changes more than the range resolution, the radar signal reflected from the target migrates to neighbouring range gates. This effect is called the range migration. The second term in (14) determines the linear part of the range migration referred to as the range walk, and the third item in (14) describes the quadratic part of the range migration known as the range curvature. What type of the migration dominates – the range walk or the range curvature – depends on the geometry of the SAR mode and the parameters involved in (14): the time of synthesis, the Doppler centroid, and the Doppler rate. An illustration of the range migration effect is given in Fig. 2.4, where a radar image is shown obtained with the discussed SAR system working as an ordinary side-looking radar (without producing the synthetic aperture) with a small (25 cm) horn antenna forming a wide beam of 8° in the azimuth. In the image, traces of migrating bright targets are clearly seen.
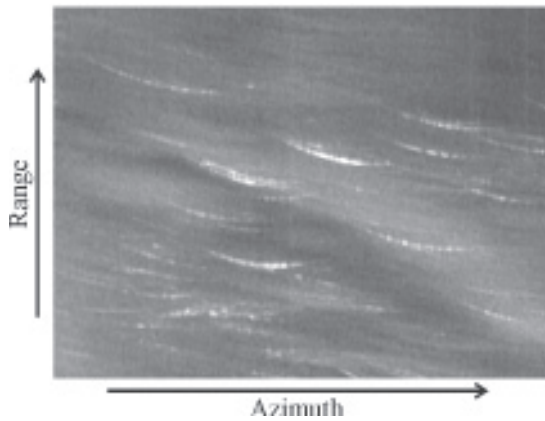
Fig. 2.4. *A side-looking radar image illustrating the range migration effect. The antenna beam width in the azimuthal direction is* $8°$

The direct solution of the range migration problem is an interpolation in a two-dimensional SAR "range-azimuth" data array along the migration curve (14). For the slant range $R_m = R_0 + m(\rho_R/2)$, where $m = 0, 1, 2, ..., M$ is the range gate index and is the slant range to the beginning of the swath strip, it is convenient to express the migration curve (14) in terms of the range gate index:

$$N_m(t) = \frac{R_m(t) - R_m(0)}{\rho_R/2} \approx \frac{\lambda}{2} \frac{F_{DC}^m t + F_{DR}^m \frac{t^2}{2}}{(\rho_R/2)}.$$

Here the upper index m indicates the particular gate number.

In Fig. 2.5 the range migration curve calculated in accordance with the above expressions is presented for two cases. Fig. 2.5,a corresponds to the case shown in Fig. 2.4, where both parts of the range migration are essential. Fig. 2.5,b illustrates the application of an antenna which forms a narrow beam of 1°. In the latter case, which is typically realized in the discussed radar, the range curvature effect is negligibly small for the time of syntheses of 1 s.

However, in spaceborne SAR systems, because of the specific geometry and a rather
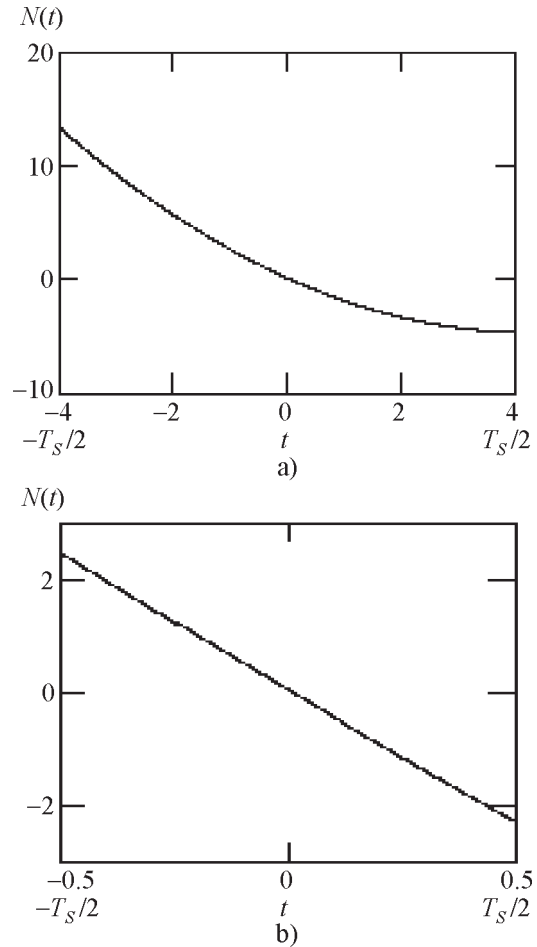

Fig. 2.5. *The theoretically calculated range migration curve for the azimuth antenna beam width of* $8°$ *(a) and* $1°$ *(b):* $\lambda = 0.02174$ *m,* $R = 2000$ *m,* $V_x = 40$ *m/s,* $H = 1500$ *m,* $\alpha = 2°$, $\beta = 5°$

long time of the synthesis, both the range walk and the range curvature usually have essential values [22-24].

During signal processing in airborne SARs, the range curvature can be neglected provided that the time of synthesis is not very long, and the Doppler rate is not very big. But the range walk in the squint SAR mode can be significant (see Fig. 2.5,b). This is particularly important for a SAR system installed on a light-weight aircraft whose orientation in space can rapidly vary in a wide range, causing large values of the Doppler centroid. If a linear frequency modulation is used for the pulse compression in range, then the linear

part of the migration can be compensated at once during the pulse compression. Moreover, special subaperture SAR processing methods were proposed for high squint angles, which allow to correct range walk inherently [22, 23].

As have already been mentioned, in the described SAR system binary phase coding is used for the pulse compression in range. Therefore, the range walk migration correction is performed by interpolating the SAR data in time domain in the two-dimensional array "range-azimuth" before the synthesis of the aperture. The need to use a pre-filter in the system imposes a limitation on the realization of the range migration correction. This filter has to be introduced, since we use a high pulse repetition frequency (up to 20 kHz) to achieve the required unambiguous speeds of ±100 m/s for moving target detection and to enhance the radar sensitivity. Such high sampling frequency is redundant for the aperture synthesis. Therefore, a pre-filtering is introduced to perform a coherent signal accumulation (taking into account currently measured Doppler centroid of the signal) and decimation from PRF to a sufficient output sampling frequency (for example, 130 Hz for 1 m resolution). The pre-filter has been designed to retain the phases of the central samples of the corresponding sums in the samples of the pre-filter output. This has been done in order to perform a correct range interpolation on decimated data for the range migration correction, accounting for the dependence of the Doppler centroid on range.

The range migration correction is performed on decimated data at the output of the pre-filter. After that the signals from all gates are convolved with a set of reference functions to synthesize the aperture. It should be noted that before applying synthesizing filter, the known Doppler centroid frequency is shifted to zero. The level of side-lobes of the synthetic aperture is about –35 dB provided that the pitch and yaw angles are within the interval ±15° and ±25°, respectively. The pre-filtering, the range migration correction, and the aperture synthesis are performed in real time.

The complex data at the output of both the synthesizing filter and the pre-filter can be stored during a flight. Since the phase history of the signals is preserved, the stored data after pre-filtering can be used for further improving quality of the SAR images by using a novel post-processing autofocusing algorithm, which is described in Section 4.

3. Compensation of the Motion Errors and Calculation of the Doppler Centroid Values

To produce undistorted high-quality, high-resolution images with an airborne SAR, it is necessary to measure accurately:
– flight altitude,
– aircraft orientation angles – pitch and yaw angles,
– aircraft velocity vector,
– aircraft acceleration vector.
The above parameters are required to calculate current values of the Doppler centroid F_{DC} and the Doppler rate F_{DR}, which are used in the SAR synthesis. These parameters are supposed to be changed slowly and considered as constant during the time of synthesis. Only the absolute, integrated aircraft trajectory is needed for an accurate ground mapping.

In order to measure the above parameters, special navigation systems consisting of an inertial navigation system and a system of GPS receivers are typically used. For an initial version of the radar, we have also developed and tested the navigation system based on the satellite orientation and positioning attitude system JAVAD AT4. This system, which is installed on an aircraft, as shown in Fig. 3.1, consists of one master-receiver and three slave GPS-receivers operating in the real-time kinematics mode relatively to the master-receiver [25]. The performed flight tests have shown that such a system does not always provide desired accuracy and reliability of the measurement of the aircraft angles. It has appeared that because of multi-path reception of GPS-signals, the accuracy can become too low for producing undistorted high-resolution SAR-images. An example of
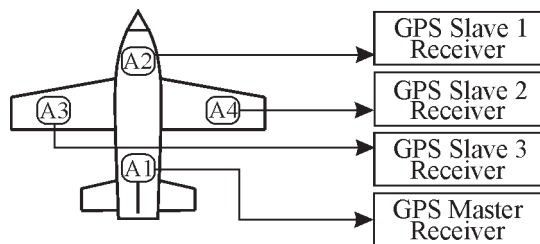
Fig. 3.1. *A way of the installation of the attitude GPS system on an aircraft*

the measurement of the pitch angle is shown in Fig. 3.2. One can see that there is a strong trend in the pitch angle evaluation with respect to the true value which for this case was equal to 0.

Another problem is related to loosing the GPS signals from the satellites due to phase locking failure during an aircraft maneuver, and a long time (from seconds to several minutes) is required for the restoration of the normal operation of the attitude determination system, which is not acceptable when a permanent earth surface monitoring is needed.

In order to overcome the problem of the orientation angles measurements, we have proposed a novel effective method of the estimation of the Doppler centroid, the aircraft orientation angles and the acceleration directly from the radar returns. In the final version of the SAR system, we have used only a simplest navigation system consisting of a single GPS receiver for measuring velocity vector and an altimeter.
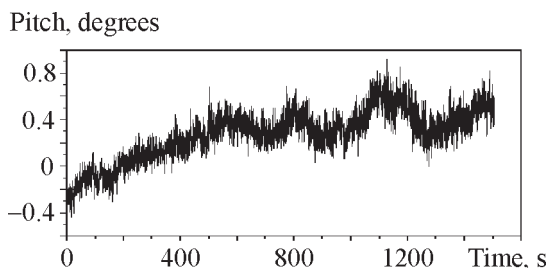
So, this navigation system provides the measurements of the coordinates, the flight height, and the velocity vector of the aircraft only.

In order to describe the proposed methods of the measurement of the orientation angles, let us go to the expression (9). Expanding this expression and taking into account the expression (4a), for the Doppler centroid we can write

$$F_{DC}^m = \frac{2}{\lambda} \frac{x_m V_x - H V_z}{R_m},$$

or

$$F_{DC}^m \frac{\lambda}{2} R_m = V_x \left[H \tan\alpha \cos\beta + \right.$$
$$\left. + \sin\beta \sqrt{R_m^2 - H^2 - (H \tan\alpha)^2} \right] - V_z H. \qquad (15)$$

In Fig. 3.3 the Doppler centroid is plotted versus the slant range for different values of the pitch and yaw angles. This figure demonstrates that there is a strong variation of the Doppler centroid on these angles. It means that there is a theoretical possibility to esti-
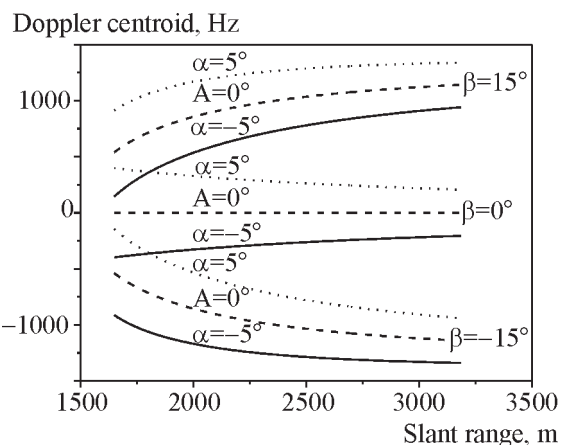
Pitch, degrees

Fig. 3.2. *Example of the pitch angle measurement with the GPS attitude system*

Doppler centroid, Hz

Fig. 3.3. *The dependence of the Doppler centroid on the slant range for different values of the pitch and yaw angles: H = 1500 m, V_x = 50 m/s, V_z = 0*

mate the orientation angles from the analysis of the dependence of the Doppler centroid on range. At the beginning of our study, the questions were: Is it possible to achieve the needed accuracy of the estimation of the orientation angles via an analysis of this dependence? And, whether it is possible to realize the corresponding algorithm in real time. Fortunately, we have found solutions which proved positive answers at the above questions.

We have found that the pitch and yaw angles, α and β, can be estimated by fitting the range dependence of the Doppler centroid to a set of Doppler centroid values $\left\{F_{DC}^m\right\}$, $m = 0, 1, 2, ..., M$ (M is the number of the range gates), roughly estimated at each range gate from the Doppler spectra. We have developed the following fast and effective fitting procedure. By introducing new variables X_m^i and Y_m as

$$X_m^i = \sqrt{R_m^2 - H^2 - \left(H \tan \alpha_{i-1}\right)^2},\qquad (16a)$$

$$Y_m = \frac{\lambda}{2}\frac{R_m}{V_x}F_{DC}^m + H\frac{V_z}{V_x},\qquad (16b)$$

equation (15) can be transformed into the equation of a straight line

$$Y_m = \left(H \tan \alpha_i \cos \beta_i\right) + X_m^i \left(\sin \beta_i\right).\qquad (17)$$

The proposed procedure is iterative with respect to the pitch angle which is considered as a small parameter. The index $i = 1, 2, ...$ is the iteration index. At the first iteration, $i = 1$, it is supposed that $\alpha_0 = 0$. At each step of the iteration, the least-mean square error fitting of the line described by (16) to the set of points $\left\{X_m^i, Y_m\right\}$ given by (17) is performed, and the orientation angles α and β are estimated. The transformation to the coordinates X_m^i and Y_m is illustrated in Fig. 3.4. The fitted curve of the Doppler dependence on range
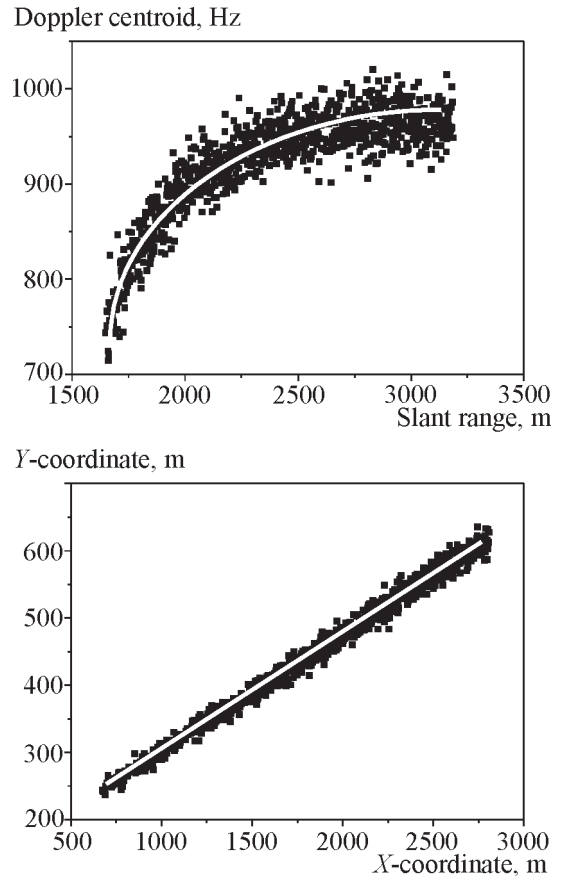

Fig. 3.4. *The transition from the original coordinates (15) to the X_m^i and Y_m^i-coordinates (17) for the Doppler centroid representation*

and the corresponding straight line are shown in the figure as well. It has been found that two iterations are typically enough to achieve an acceptable accuracy of the estimated angles. As soon as the orientation angles are found, the Doppler centroid can be calculated from (3) and (5). The procedure of fitting the straight line to a set of point is very simple and does not require much computation.

In contrast to known Doppler centroid estimation techniques [28, 29], for which the dependence of the Doppler centroid on range is undesirable, the described method effectively exploits this dependence.

The described technique of the estimation of the orientation angles and the calculation of Doppler centroid values is fast enough to

be realized in real time. The method was successfully introduced in a real-time signal processing system of the discussed airborne SAR [5, 26, 27]. In Fig. 3.5, an example of the Doppler centroid range dependence measured during a flight is depicted. Due to bright targets Doppler centroid estimated directly from the spectrum on each range gate has a noisy bias from true value. Besides that, there are a number of gates where the reflected signal was weak and the estimation of the Doppler centroid has a valuable error. Nevertheless, the Doppler centroid values estimated in accordance with the above described algorithm fit good the measured values, as one can see from this figure.

The proposed method of the pitch and yaw angles estimation has appeared to be rather robust and efficient. At the same time, it provides a high accuracy of the angles estimation, which is about 0.1°. Taking into account that the antenna beam width in our case is about 1°, such accuracy is quite enough to realize a high quality image synthesis. Our computer simulations and experimental results indicate that the allowable values of the pitch and yaw angles are $\alpha = \pm 15°$ and $\beta = \pm 25°$, correspondingly. The sampling rate of the angle estimation in the SAR system is about 20 Hz, while the time of the aperture synthesis is about 1 s.
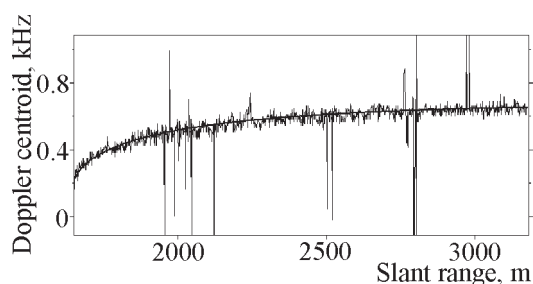

Fig. 3.5. *The thin line is the Doppler centroid range dependence measured in real-time on reflected signal spectra. The thick line shows the estimated Doppler centroid range dependence (15) after estimation of the pitch α and yaw β angles*

4. Autofocusing by Estimating the Aircraft Acceleration

In order to obtain well-focused SAR images, the Doppler rate (9) should be calculated with a high accuracy. The estimation of the Doppler rate directly from the radar returns, called autofocusing [29-31], provides better accuracy than the calculation, which is based on sensor data only [1, 2, 29]. Expanding (9), we find for the Doppler rate, F_{DR},

$$F_{DR}^m = -\frac{2}{\lambda}\left[\frac{1}{R_m}\left(\left(V_x^2 + V_z^2\right) - \frac{\left(x_m V_x - H V_z\right)^2}{R_m^2}\right) - \right.$$

$$\left. - \frac{\left(x_m A_x + y_m A_y - H A_z\right)}{R_m}\right]. \tag{18}$$

One can see that the only unknown parameter is the acceleration vector, given that the orientation angles and the velocity vector have been estimated.

During the on-board, real time signal processing, the focused SAR images are built assuming zero acceleration. However, as has already been mentioned, in the discussed SAR system there is a possibility to save complex data after pre-filtering and decimation (and even raw data) during a flight. This provides additional opportunities for post-processing of the radar images.

In general case, it is possible to assume that the along-track component of the acceleration, A_x, is compensated. This can be done, for example, by slaving the pulse repetition frequency, F_{PRF}, in order to keep the ratio V_x/F_{PRF} constant, supporting $A_x = 0$. To estimate the unknown across-track components of the acceleration, A_y and A_z, we have proposed an autofocusing technique, which is a combination of the contrast optimization technique [2, 3] and the multi-look registration method [2].

According to the contrast optimization technique [2], the same part of a SAR image is synthesized by using different values of the Doppler rate. It is assumed that the usage of

the correct Doppler rate value results in the image with a maximum contrast. The local variance of the image can be used as a measure of the contrast. This method works well on image segments which have contrast image features and may failure on uniform regions filled with speckle.

The multi-look registration method [2] consists in the following. The whole interval of the synthesis is divided into several parts (for example, 3 or 5), and then several independent images of the same ground patch are formed. These images have worse resolution and are called "looks". If the used Doppler rate for the synthesis is incorrect, then these images will be shifted to each other. According to the multi-look registration method, these shifts are estimated and used to determine a correct value of the Doppler rate. If the SAR aircraft motion is unstable, the Doppler rate strongly depends on range and azimuth, and the shifts will be different at each point of the SAR image, and the application of this approach is problematic.

According to the proposed technique, which can be called the strip-map multi-look contrast optimization technique, the contrast is calculated on a multi-look image obtained by summation of independent looks. In such approach, the maximum contrast is obtained not only when contrast features are focused well on each look (the contrast optimization aspect), but also when the independent looks are summed up without shifts (the multi-look registration aspect). In addition, the contrast is calculated on the multi-look image, on which speckle noise is reduced due to non-coherent averaging [1, 2]. Moreover, during such contrast optimization we vary the acceleration rather than the Doppler rate itself, accounting in this way for the dependence of the Doppler rate on range. Therefore, for the contrast estimation, it is possible to choose the most contrast parts of the range line within the whole swath width. Such peculiarities of the proposed technique make the estimation more stable and reliable. When the acceleration is found, the Doppler rate values are calculated for each range gate by using (18).

The proposed strip-map multi-look contrast optimization technique still has the following difficulty. During the contrast optimization, it is necessary to estimate two across-track components of the acceleration: A_y and A_z. It has appeared that this problem can be solved out as well. One should note that the component A_y appears in (18) with the coefficient, which depends on range, while the component A_z appears with the coefficient, which does not depend on range:

$$\left(\mathbf{R}_m \cdot \mathbf{A}\right) = y_m\left(R_m\right)A_y - HA_z.$$

This fact is illustrated in Fig. 4.1, where the dependence of the Doppler rate on range is shown for different combinations of the acceleration components.

Performing the autofocusing by assuming $A_y = 0$ in the near and in the far $1/3$ of the swath independently, then the estimated values of the acceleration, A_{zNear} and A_{zFar}, can be used to separate the two across-track components of the acceleration by solving the following system of linear equations:
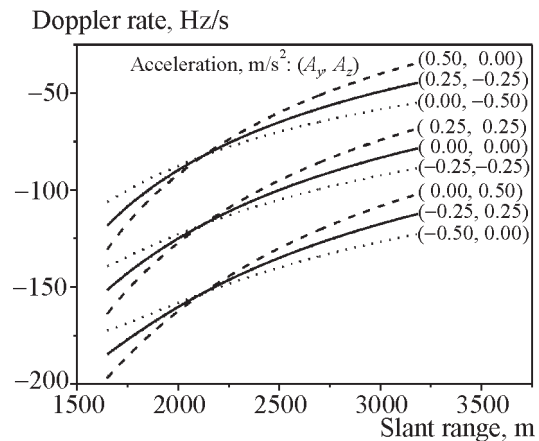

Fig. 4.1. *The range dependence of the Doppler rate for different values of acceleration components A_y and A_z: $H = 1500$ m, $V_x = 50$ m/s, $V_z = 0$, $\alpha = 0$, $\beta = 0$*

$$A_z - A_y \left[\frac{1}{H} \frac{1}{M/3} \sum_{m=2M/3}^{m=M} y_m \right] = A_{z\,Far},$$

$$A_z - A_y \left[\frac{1}{H} \frac{1}{M/3} \sum_{m=1}^{m=M/3} y_m \right] = A_{z\,Near}.$$

It should be noted that in the most known autofocusing techniques [29, 30] the dependence of the Doppler rate on range is undesirable. Here, similar to the Doppler centroid estimation method (see Section 3), we effectively exploit this dependence. The described method of autofocusing has appeared to be rather robust and accurate. The accuracy of the acceleration estimation is about 0.05 m/s^2. However, so far realization of this method requires essential computational resources, and it was introduced as a post-processing algorithm. The method was successfully tested for post-processing of the radar data recorded during flight experiments with the airborne SAR [4, 5, 26, 27]. In Section 6, the results of the method application are discussed.

5. Radar System Hardware

A simplified block-diagram of the radar system is shown in Fig. 5.1 and the main radar characteristics are summarized in Table 1. The radar transmitter is based on a TWT amplifier operating in a recuperation regime. An efficient high voltage power supply produces all needed voltages and contains circuits to provide both monitoring of transmitter critical parameters and safe operation of the TWT. A high voltage solid state modulator is used to produce a required voltage swing across the TWT control grid. The transmitter circuits are controlled by a microcontroller which communicates with the radar host computer.

The receiver uses one frequency conversion with the intermediate frequency of 400 MHz. It contains a digitally controlled attenuator for extending the receiver dynamical range. The receiver protection circuitry is designed by using a circulator along with a P-i-N modulator. It also contains a noise source coupled to the receiver input for calibrating the receiver sensitivity.
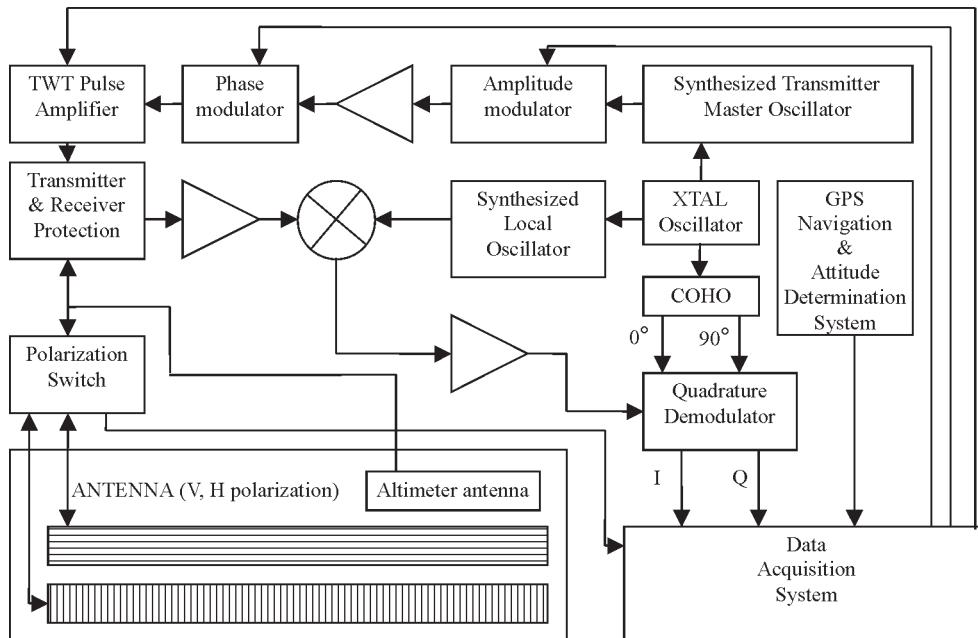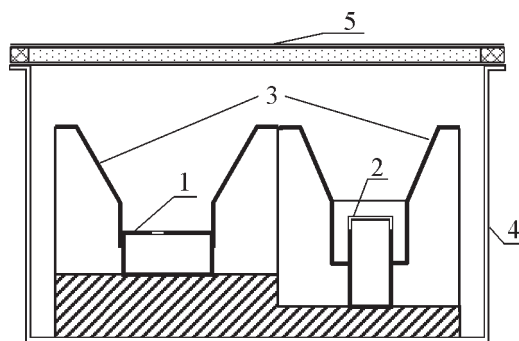

Fig. 5.1. *Simplified functional block diagram of the radar transmitter-receiver module*

Table. 5.1. *The main radar hardware characteristics*

Transmitter specifications	
Operating frequency	Ku-band
Transmitter pulse output power, W	120
Platform velocity, m/s	$30 \div 100$
Pulse repetition rate, Hz/(m/s)	≤ 200
Pulse duration, μs	5.12
Pulse compression	Binary phase coding
Pulse compression length	255
Receiver specifications	
Receiver noise figure, dB	2.5
System loss (Tx+Rx side), dB	$(3.1 + 0.9) = 4.0$
I, Q bandwidth, MHz	50
ADC dynamic range, dB	36
Antenna specifications	
Type	Slotted waveguide
Antenna length, m	1.8
Azimuth beam width	1°
Elevation beam width	40°
Gain, dB	30
Polarization	Horizontal and vertical
Polarization decoupling, dB	>40

Fig. 5.2. *Cross-section of the antenna system: 1 – waveguide-grating for the vertical polarization; 2 – waveguide-grating for the horizontal polarization; 3 – 2-D horns; 4 – antenna airframe; 5 – radome*

In the radar, two separate antennas are introduced – for horizontal and vertical polarizations, respectively. We have used two types of the radar antenna systems: a horn and a waveguide-slot grating. The horn antenna is rather compact with a maximum dimension of 25 cm so as to simplify its installation on an aircraft. In order to increase the accuracy of moving target detection and to increase the radar potential, a waveguide-slot antenna has also been developed and tested. The antenna cross-section is shown in Fig. 5.2. There are two antenna gratings: one with axial slots in the wide waveguide wall, and the second with transverse slots in the narrow waveguide wall for the vertical and horizontal polarization, respectively. The antenna pattern in the tilt direction is formed by 2-D horns made of metallic plates. The antenna system is protected by a radome, which has a multi-layer structure. The radome is made of composite materials used in aircraft constructions. The power losses in the radome are as low as 0.2 dB. The antenna system is connected to the transmitter-receiver module via a p-i-n modulator.

The radar data acquisition system contains dual-channel, high-speed ADCs, FPGA, and DSP along with SRAM and DRAM modules. The following functions are realized in FPGA: pulse compression, fast Fourier transformation (FFT) for moving target indication (MTI) and rough estimation of Doppler centroid values, pre-filtering with the Doppler centroid compensation, and the focused aperture synthesis with the range migration correction. The DSP performs the following functions: accurate, real-time estimation of the pitch and yaw angles, calculation of the Doppler centroid and Doppler rate values, and final processing for MTI.

The signal processing starts from data digitizing and pulse compressing along range. After that, by using the FFT with the length of 1024 (along the azimuth), the Doppler spectra of the signal for each gate are calculated. By using these spectra, a rough estimation of the central Doppler frequencies for each gate is performed and moving targets, if any, are detected. Next, the antenna beam orientation angles are estimated by using the pro-

posed method (see Section 4), and the Doppler centroid and the Doppler frequency rate are calculated along with the reference functions. Then, the coherent signal accumulation and data decimation are performed in the preliminary filter. The range migration correction and the aperture synthesis are performed on the decimated data in real-time by using the method of direct convolution in the time domain. During flight, the decimated data after pre-filtering along with real-time synthesized image can be on-the-fly viewed on the monitor screen and stored on a hard disk drive of the radar host computer. The stored decimated data are suitable for the following multi-look and autofocusing post-processing, as described in the previous section. The specifications of the flight geometry and real-time data processing are gathered in the Table 5.2.

6. Flight Tests

An important advantage of the developed SAR system is related with the possibility of its operation from small platforms. A number of flight tests with the system have been performed. In particular, the SAR system was installed on a light-weight, single-engine biplane Antonov AN-2 as shown in Fig. 6.1,a. For the permanent exploitation, the radar was installed on the turbo-prop engine aircraft Y-12 (see Fig. 6.1,b). In all of flight tests, the radar has demonstrated a high reliability, and only a couple of first flight tests were needed to adjust the image and MTI processing algorithms along with the methods of the estimation of the Doppler centroid values in real time.

An example of a real-time SAR image with the detection of moving targets, which are cars on roads, is presented in Fig. 6.2. Figure 6.3 illustrates another scene with the MTI processing. Moving targets are detected via the analysis of Doppler frequencies which are different from the Doppler frequencies of the ground clutter as described in Section 2.3. As one can see, moving targets are detected easily in the Fourier domain and then placed on the corresponding SAR focused image (see

Fig. 6.2. and 6.3,b). Such targets, separated from the ground clutter are shown in Fig. 6.3,a. Colour palette is used to indicate value of the Doppler velocity and its direction. As mentioned in Section 3, the signals, which correspond to moving targets, do not pass through the synthesizing filter. Therefore, the azimuth target position on a SAR image corresponds to the orientation of the antenna beam maximum in the azimuth direction. The experiments have proved a reliability and robustness of such simple method of moving target detection.

In most cases the quality of real-time radar images are sufficient for a number of applications. However, when the platform motion is rather unstable, for example, because of turbulence or strong wind, real time images are not so nice and additional signal processing is needed. Furthermore, a single-look SAR image is always corrupted by speckle noise. The quality of the images can be improved by using the strip-map multi-look contrast optimization autofocusing technique proposed in Section 4.

In Fig. 6.4, an example of SAR image with the resolution of 3×3 m after autofocusing processing is presented. In Fig. 6.5,a, a part of this image before autofocusing is shown. In the middle of the image one can see a blurring vertical strip which is a result of abrupt instability of the flight at that moment. To correct this defect, the proposed autofocusing technique was applied. After its application, the blurring vertical strip was completely removed, and the complete radar image was focused perfectly as well (see Fig. 6.5,b).

In Fig. 6.6,a, another real-time single-look focused SAR image obtained during a strongly unstable flight is shown. The image was formed assuming $A_y = 0$ and $A_z = 0$, i. e. without autofocusing. An attempt to improve the quality of this image by using just the multi-look processing without autofocusing is shown in Fig. 6.6,b. One can see that the result is quite opposite – the image becames more blurred. This is because the usage of a wrong focusing coefficient that leads to a displacement of the separate looks.
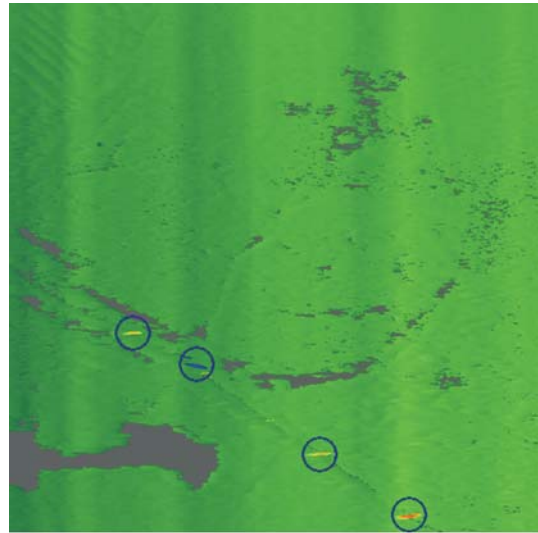
Table. 5.2. *Specifications of the flight geometry and real-time data processing*

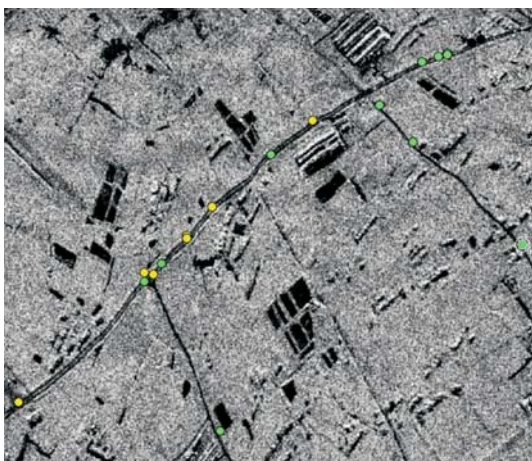| Specifications of the flight geometry and data processing	
ADC sampling rate, MHz	100
ADC resolution, bit	12
Number of range gates	1024
Slant range resolution, m	3
Azimuth resolution, m	from 1 to 6
Flight height, m	typically 2000
Incidence angles	from 15° to 55°
Near range (on ground map), m	500
Far range (on ground map), m	3000
Swath width, m	2500
Real-time processing	Full resolution
Yaw angle	$< 25°$
Pitch angle	$< 15°$
Accuracy of embedded altimeter, m	5
Accuracy the angles auto-estimation	0.1°
Accuracy of the velocity vectors estimation by GPS measurements, m/s	0.02 (satellites >6)
Recording and imaging output data	
Data transfer rate, Mbps	650
Recorded data	Radar data: raw data (range compressed without azimuth compression) or processed data (after pre-filter and focused SAR image data) MOCO: orientation angles, velocity, 3D-position Debug: ADC output/range compressed data/Doppler centroid
Displayed data	After pre-filter and focused SAR image (256 gray levels)
PSLR, dB	−30
ISLR, dB	−27
Image size (visible scrolling part of the strip)	1024×1024 pixels, 1536 m on slant range, 500÷2500 m on azimuth (depends on resolution)
Moving targets detection and imaging	
Unambiguity velocity range, m/s	−100÷100
Velocity estimation accuracy, m/s	0.2
Moving target position accuracy, m	3 (on range), 10 (on azimuth)
Ground clutter rejection, dB	>25

a)

b)

3 × 3 m

Fig. 6.1. *Flight tests: a) radar system installed on single-prop engine biplane Antonov AN-2 (Korotich, Ukraine); b) radar system installed on turbo-prop engine aircraft Y-12 (Changzhou, China)*

a)

b)

Fig. 6.3. *MTI processing: a) Doppler centroid gray level map; b) corresponding SAR image (AN-2 aircraft, resolution) with the moving targets*

Fig. 6.2. *Example of SAR image with moving targets detection (Y-12 aircraft, 5 × 3 m resolution)*

To solve this problem, the proposed multi-look contrast optimization, autofocusing technique can be used to obtain a well-focused image. The result of its application is shown in Fig. 6.6,c for the single-look image. One can see that now bright points are accurately focused as well as other image details. The result of the application of the multi-look pro-
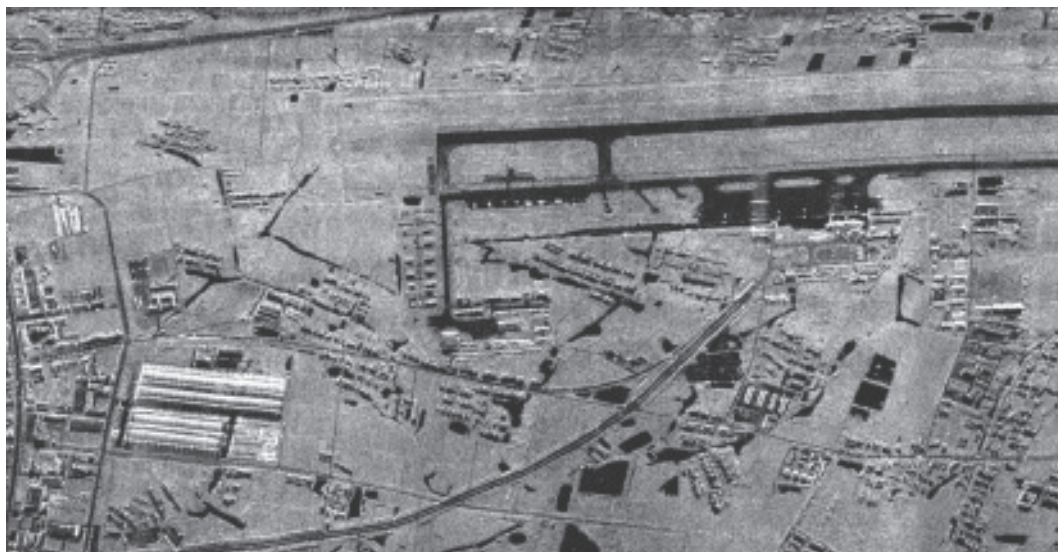
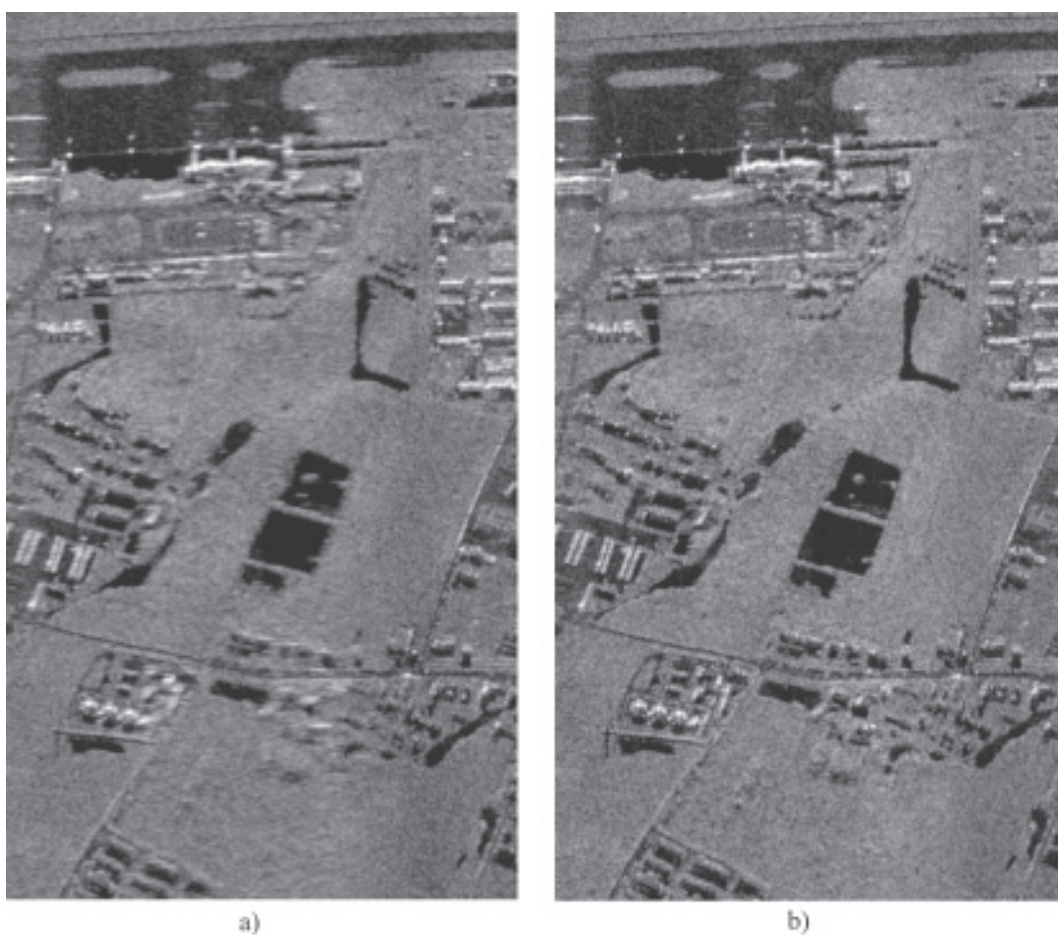**Fig. 6.4.** *Example of the autofocused SAR image (Y-12 aircraft, $3 \times 3\,m$ resolution)*

a)   b)

Fig. 6.5. *Autofocusing of the SAR image (Y-12 aircraft, $3 \times 3\,m$ resolution): a) before autofocusing; b) after autofocusing*
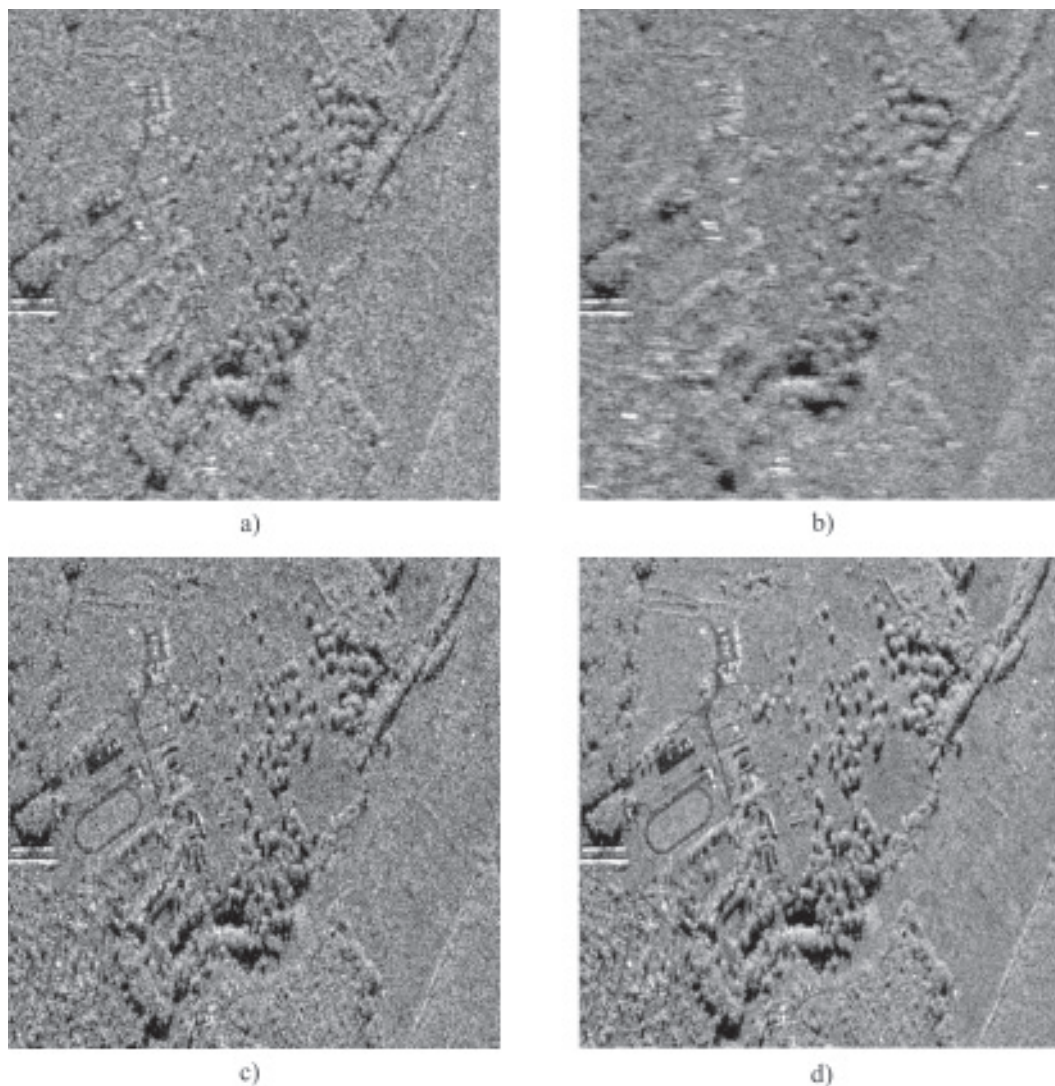
Fig. 6.6. *Illustration of multi-look and autofocusing post-processing (AN-2 aircraft, 3×3 m resolution)*

cessing is shown in Fig. 6.6,d, where a three-look image is shown. A notable reduction of the speckle noise as compared to the pervious image is seen here.

7. Conclusion

In this paper, we have described a recently developed Ku-band airborne SAR system. The SAR system is cost-effective due to the following solutions introduced: a simple navigation system combined with real-time estimation of the pitch and yaw angles, a pulse compression with binary phase coding, a specific pre-filte-ring procedure, and a multi-look autofocusing. The SAR system can be effectively operated from small aircrafts. Capabilities of the system are enhanced due to the possibilities to perform measurements at two polarizations and to indicate moving targets. Flight tests have proved high effectiveness and reliability of the solutions introduced in the system.

References

1. F. T. Ulaby, R. K. Moore, and A. K. Fung, *Microwave Remote Sensing, Active and Passive.* Vol. II. Reading, Mass.: Addison Wesley, 1983.
2. Chris Oliver and Shaun Quegan, *Understanding Synthetic Aperture Radar Images.* Boston, London: Artech House, 1998.
3. C. J. Oliver, "Synthetic-aperture radar imaging", *J. Phys. D: Appl. Phys.*, vol. 22, pp. 871-890, 1989.
4. D. M. Vavriv, V. V. Vynogradov, V. A. Volkov, R. V. Kozhyn, O. O. Bezvesilniy, S. V. Alekseenkov, A. V. Shevchenko, and M. P. Vasilevskiy, "Cost-effective Ku-band airborne SAR with indication of moving targets", in *Proc. International Radar Symposium IRS 2005*, Berlin, Germany, 2005, pp. 203-207.
5. D. M. Vavriv, V. V. Vynogradov, V. A. Volkov, R. V. Kozhyn, O. O. Bezvesilniy, S. V. Alekseenkov, A. V. Shevchenko, and M. P. Vasilevskiy, "Cost-effective Ku-band airborne SAR with Doppler centroid estimation, autofocusing and indication of moving targets", in *Proc. EuRAD*, 2005.
6. D. G. Thompson, D. V. Arnold, D. G. Long, G. F. Miner, M. A. Jensen, T. W. Karlinsey, A. E. Robertson, J. S. Bates, "YSAR and YINSAR: Compact, Low-Cost Synthetic Aperture Radars", in *Proc. European Conference on Synthetic Aperture Radar*, Friedrichshafen, Germany, 25-27 May, 1998, pp. 27-30.
7. G. Fornaro, "Trajectory Deviations in Airborne SAR: Analysis and Compensation", *IEEE Transactions Aerospace Electronics Systems*, vol. 35, No. 3, pp. 997-1009, July 1999.
8. S. Buckreuss, "Motion Errors in an Airborne Synthetic Aperture Radar System", *ETT Journal*, vol. 2, No. 6, pp. 655-664, Nov.-Dec. 1991.
9. A. Moreira, Y. Huang, "Airborne SAR Processing of High Squinted Data Using a Chirp Scaling Approach with Integrated Motion Compensation", *IEEE Transactions Geoscience Remote Sensing*, vol. 32, No. 5, pp. 1029-1040, Sep. 1994.
10. J. R. Moreira, "A new method of aircraft motion error extraction from radar raw data for real time motion compensation", *IEEE Transactions Geoscience Remote Sensing*, vol. 28, No. 4, pp. 620-626, Sep. 1990.
11. Nadav Levanon and Eli Mozeson, *Radar signals.* John Wiley & Sons Inc., 2004.
12. A. M. Boehmer, "Binary Pulse Compression Codes", *IEEE Transactions Information Theory*, vol. IT-13, No. 2, pp. 156-167, April 1967
13. *Sovremennaya radiolokatsiya. Analiz, raschet i proektirovanie sistem.* Moskow: Sovetskoe Radio, 1969, 704 p. (In russian)
14. R. K. Raney, "Synthetic aperture imaging radar and moving targets", *IEEE Transactions Aerospace Electronics Systems*, vol. 7, No. 3, pp. 499-505, 1971.
15. *Radar Handbook*. Ed. M. I. Skolnik. New York: McGraw-Hill, 1990.
16. M. Soumekh, "Moving target detection in foliage using along track monopulse synthetic aperture radar imaging", *IEEE Transactions Image Processing*, vol. 6, No.8, pp. 1148-1163, 1997.
17. M. Soumekh, and B. Himed, "Moving target detection and imaging using an X-band along-track monopulse SAR", *IEEE Transactions Aerospace Electronics Systems*, vol. 38, No. 1, pp. 315-333, 2002.
18. Moccia A., and Rufino G. "Spaceborne along-track SAR interferometry: performance analysis and mission scenarios", *IEEE Transactions Aerospace Electronics Systems*, vol. 37, No. 1, pp. 199-213, 2000.
19. Klemm R. "Adaptive clutter suppression for airborne phased array radars", *IEE Proceedings, Part F*, vol. 130, No. 1, Feb. 1983, pp. 125-132.
20. Klemm R. "Space-Time Adaptive Processing: principles and applications", *IEE*, London, 1998.
21. Ward, J. "Space-time adaptive processing for airborne radar", *Technical Report No. 1015*, Lincoln Laboratory, MIT, Dec. 1994.
22. T. S. Yeo, N. L. Tan, Ch. B. Zhang, "A new sub-aperture approach to high squint SAR processing", *IEEE Transactions Geoscience Remote Sensing*, vol. 39, No. 5, pp. 954-967, May 2001.
23. M. Y. Jin, Ch. Wu, "A SAR correlation algorithm which accommodates large-range migration", *IEEE Transactions Geoscience Remote Sensing*, vol. GE-22, No. 6, pp. 592-597, Nov. 1984.
24. Ch. Wu, K. Y. Liu, M. Jin, "Modeling and a Correlation Algorithm for Spaceborne SAR signals", *IEEE Transactions Aerospace Electronics Systems*, vol. AES-18, No. 5, Sep. 1982, pp. 563-574.
25. L. Rapoport, I. Barabanov, A. Khvalkov, A. Kutuzov, J. Ashjaee. "OCTOPUS: Multi antennae GPS/GLONASS RTK System", in *Proc. ION GPS-99 Meeting*, Nashville, Tennessee, 1999.
26. O. O. Bezvesilniy, V. V. Vynogradov, and D. M. Vavriv. "Estimating Doppler centroid and autofocusing for airborne SAR", in *Proc. International Radar Symposium IRS*, Berlin, Germany, 2005, pp. 59-63.
27. O. O. Bezvesilniy, D. M. Vavriv, V. V. Vynogradov, "Otsenivanie doplerovskogo tsentroida i avtofocusirovka v samoletnom radiolokatore bokovogo obzora s sintezirovannoi aperturoi", *Doklady NAN Ukrainy*, № 9, 2005, pp. 77-83 (in russian).
28. S. Madsen, "Estimating the Doppler centroid of SAR data", *IEEE Transactions Aerospace Elec-*

tronics Systems, vol. AES-25, No. 2, pp. 134-140, March 1989.

29. F. -K. Li, D. N. Held, J. C. Curlander, and C. Wu, "Doppler parameter estimation for spaceborne synthetic-aperture radar", *IEEE Transactions Geoscience Remote Sensing*, vol. GE-23, No. 1, pp. 47-56, Jan 1985.

30. E. Wahl, P. H. Eichel, D. C. Ghiglia, and C. V. Jakowatz Jr., "Phase gradient autofocus – a robust tool for high resolution SAR phase correction", *IEEE Transactions Aerospace Electronics Systems*, vol. AES-30, No. 3, pp. 827-835, July 1994.

31. D. G. Thompson, J. S. Bates, D. V. Arnold, "Extending the Phase Gradient Algorithm for Low-Altitude Stripmap Mode SAR", in *Proc. International Geoscience and Remote Sensing Symposium*, IGARSS, 28 June - 2 July, Hamburg, Germany, 1999.

Недорогой эффективный самолетный РСА

Д. М. Ваврив, В. В. Виноградов, В. А. Волков, Р. В. Кожин, А. А. Безвесильный, С. В. Алексеенков, А. В. Шевченко, А. А. Беликов, М. П. Василевский, Д. И. Заикин

Самолетный радиолокатор Ku-диапазона с синтезированной апертурой (РСА), разработанный и прошедший испытания в Радиоастрономическом институте НАН Украины, является недорогой эффективной системой с точки зрения ее разработки и эксплуатации. Данный РСА может быть установлен на легкомоторном самолете и позволяет получать радиолокационные изображения с высоким разрешением в реальном масштабе времени. Важным достоинством системы является реализация оригинального алгоритма определения углов ориентации самолета в реальном времени, основанного на анализе отраженных от земли сигналов. В статье описаны принципы действия разработанного РСА, устройство и основные компоненты системы, алгоритмы обработки сигналов, а также приведены результаты экспериментальных полетов с использованием системы РСА.

Недорогий ефективний літаковий РСА

Д. М. Ваврів, В. В. Виноградов, В. А. Волков, Р. В. Кожин, О. О. Безвесільний, С. В. Алексеєнков, О. В. Шевченко, О. О. Бєліков, М. П. Василевський, Д. І. Заікін

Літаковий радіолокатор Ku-діапазону з синтезованою апертурою, що був розроблений та пройшов випробування в Радіоастрономічному інституті НАН України, є недорогою ефективною системою з точки зору її розробки та експлуатації. Такий РСА можна встановити на невеликому літаку і мати можливість отримувати радіолокаційні зображення з високим розрізненням у реальному часі. Важливою перевагою цієї системи є оригінальний алгоритм визначення кутів орієнтації літака у реальному часі, що базується на аналізі сигналів, відбитих від поверхні землі. У статті наводяться принципи дії розробленої системи РСА, її будова та головні компоненти, алгоритми обробки сигналів, а також результати експериментальних польотів з використанням системи РСА.